Hindawi
Mathematical Problems in Engineering
Volume 2022, Article ID 3588068, 15 pages
https://doi.org/10.1155/2022/3588068

Research Article

Hopf Bifurcation of a Standing Cantilever Pipe Conveying Fluid with Time Delay

Cheng Feng,[1] Yun-dong Li ,[1] and Gui-yu Ou[2]

[1]*School of Mathematics and Statistics, Sichuan University of Science and Engineering, Zigong 643000, China*
[2]*Sichuan Province University Key Laboratory of Bridge Non-Destruction Detecting and Engineering Computing, Zigong 643000, China*

Correspondence should be addressed to Yun-dong Li; lyd1114@126.com

Received 29 September 2022; Revised 24 November 2022; Accepted 6 December 2022; Published 24 December 2022

Academic Editor: Lei Hou

In this article, the dynamical behavior of a standing cantilever pipe conveying fluid is investigated with time − delay. By applying piezoelectric materials and considering the time delay of voltage, the motion equation is built with motion-limiting constraints and elastic support. The motion equation is discretized into ordinary differential equations by the Galerkin method. A stability analysis of the equilibrium point with three parameters is obtained. The system will lose stability at the equilibrium point and generate Hopf branches. The central manifold theorem and the canonical type theory are used to study the stability of Hopf branching directions and branching period solutions. Finally, numerical results validate the theoretical analysis.

1. Introduction

Pipes conveying fluid can be found in some engineering structures, such as submarine oil pipelines, fuel delivery pipelines for aircraft, and heat exchange systems for nuclear power plants. The fluid flowing in the pipe will cause vibration problems of pipe. Long-term vibration will cause safety problems for the structure. Based on the safety problems, the vibration of pipes conveying fluid is one of the hot spots studied by a lot of scholars. Therefore, there have been a number of studies on the stability of pipes conveying fluid in the past decades. By analyzing the linear model of pipe conveying fluid, Paidoussis [1] found two noteworthy instabilities: divergence instability and flutter instability. A pipe conveying fluid with support at both ends shows the divergence instability beyond a critical flow velocity, and a cantilever pipe conveying fluid has flutter instability beyond a critical flow velocity. Especially, vibration research of cantilever pipe conveying fluid has aroused great interest among some scholars. By considering constraint conditions in a linear model, Païdoussis et al. [2, 3] studied the stability and chaotic motion of a cantilevered pipe conveying fluid under three times nonlinear spring constraints. Jin [4] investigated the stability and dynamics of a cantilevered pipe conveying fluid with motion-limiting constraints and an elastic support and showed the effect of the spring constant and some other parameters on the dynamics of the system. Wang and Ni [5] developed the research results of Jin and presented the stability and chaotic motions of a standing pipe conveying fluid that is studied and further compared with that of a hanging system. Based on a novel extended version of the Lagrange equations for systems containing nonmaterial volumes, Stangl et al. [6] deduced the nonlinear equations of motion for cantilever pipe systems conveying fluid. An alternative to existing methods utilizing Newtonian balance equations or Hamilton's principle is thus provided. Ghayesh et al. [7] studied the nonlinear planar dynamics of a fluid-conveying cantilevered pipe. The extended version of the Lagrange equations for systems containing nonmaterial volumes is employed to derive the equations of motion, resulting directly in a set of coupled nonlinear ordinary differential equations. The pseudoarclength continuation technique along with direct time integration is used to solve these equations. Liu et al. [8] explored the nonlinear forced vibrations of a cantilevered pipe conveying fluid under base excitations by means of the full nonlinear equation of

motion. The self-excited vibration is briefly discussed, focusing on the effect of flow velocity on the stability and postflutter dynamical behavior of the pipe system with parameters close to those in previous experiments.

It should be noted that a Hopf bifurcation would arise when the cantilever pipe conveying fluid system is unstable. Hopf bifurcation is an essential part of the qualitative theory of dynamical systems, which is widely used in nature and engineering, such as biology, mechanics, and artificial intelligence. Many scholars have contributed to studying the Hopf bifurcation problem in cantilevered pipes conveying fluid. Bajaj et al. [9] investigated the self-induced planar nonlinear oscillations of a cantilever tube carrying an incompressible fluid. When the zero solution becomes unstable by a pair of complex conjugate eigenvalues of the linearized system crossing the imaginary axis, the system satisfies conditions for Hopf bifurcation and the zero solution bifurcates into periodic orbits. The bifurcated periodic solutions are determined using center-manifold and averaging ideas. In the literature [10–13], the nonlinear response characteristics of a cantilevered pipe conveying fluid with a spring support and nonlinear motion constraint and the bifurcation behavior of the system near the double degradation point were investigated. Modarres-Sadeghi et al. [14] investigated the two-dimensional (2-D) and three-dimensional (3-D) flutter of cantilevered pipes conveying fluid. Yamashita et al. [15] investigated the dynamics of a pipe with a spring support and an end mass. They focus on Hopf-Hopf interactions and conduct nonlinear analyses to clarify the evolutions of the amplitudes of two unstable modes. In a certain range of the parameters, there are mixed-mode self-excited vibrations, which are produced by the Hopf-Hopf interactions.

Active control of the vibration is necessary to reduce the hazards associated with cantilever pipe conveying fluid. With the development of material science, the preparation technology of smart materials such as piezoelectric materials tends to mature, making the cost of vibration control based on piezoelectric gradually reduced. Therefore, discussions on piezoelectrically driven cantilever pipes conveying fluid have drawn serious attention. Lin and Chu [16] used state-of-the-art piezoelectric ceramics as the actuators for active flutter suppression of a cantilever tube transporting high-speed moving fluid. The flutter vibration of the cantilever tube can be effectively suppressed with the moderate driving control voltage fed into the piezoelectric actuators. Tsai and Lin [17] designed a model reference adaptive control method in modal space for flutter control of a cantilevered pipe conveying fluid. The control input is provided by a pair of surface-mounted piezoelectric actuators which are driven 180° out of phase to provide an equivalent bending moment acting on the controlled system. Active flutter control of a thin-walled functionally graded piezoelectric (FGP) cantilever pipe via optimal control law was investigated by Fazelzadeh and Yazdanpanah [18]. A linear quadratic regulator (LQR) controller is employed in order to suppress the unwanted vibration caused by the system's flutter. Abbasnejad et al. [19] presented the stability analysis of a fluid-conveying micropipe axially loaded with a pair of piezoelectric layers located at its top and bottom surfaces. Taking into account clamped-free boundary conditions with and without intermediate support, the stability of the system is investigated to demonstrate the influence of flow velocity as well as the voltage of the piezoelectric layers on the flow-induced flutter instability. Wang and Shen [20] developed a nonlinear model for a cantilevered piezoelectric pipe conveying fluid that included geometric nonlinearity and electromechanical coupling. Due to the presence of piezoelectric materials, the critical flutter velocity depends on resistive piezoelectric damping and electromechanical coupling. Dai et al. [21] employed a kind of large deformations induced by nonlinear vibrations of a soft pipe conveying fluid to design an underwater bio-inspired snake robot that consists of a rigid head and a soft tail. The research provided a new thought to design driving devices by using nonlinear flow-induced vibrations.

The time delay inevitably exists in active control systems. In the control system of pipe conveying fluid, the time delay may be utilized to enhance the critical flow velocity. The study of time-delay dynamical systems has essential theoretical and practical significance. Some dynamical phenomena can only be explained reasonably when the time delay is considered. For example, when negative feedback is introduced in a cantilever beam to increase the damping of the system, it is not the case that the greater the feedback gain, the better the stability of the system. When the feedback gain reaches a specific amount, the system will exhibit strong self-excited vibration under a specific initial disturbance. This phenomenon is difficult to explain without considering the effect of time delay. On the other hand, the time delay can also be exploited to improve the performance of control systems. For example, time-delay feedback control is one of the main methods to control chaos in dynamical systems. Sugimoto et al. [22] added a compensator to the time-delay controller, which made the stability and other performance of the time-delay controller better than the traditional time-delay controller. The phase lag caused by the delay link is compensated to some extent. For dual-input dual-output linear time-delay systems, Mirkin and Gutman [23] proposed an output feedback control scheme and adaptive rate based on MRAC, which can make the error asymptotically approach zero. Qi and Xu [24] investigated the relationship between time delay and critical flow velocity of cantilevered pipe conveying fluid under a time-delay control strategy. They achieved the purpose of increasing the critical flow velocity by actively adjusting the time delay. Wang and Ni [25] investigated the Hopf bifurcation and chaotic motions of a tubular cantilever impacting on loose support by using an analytic model that involves delay differential equations. By using the damping-controlled mechanism, a single flexible cantilever in an otherwise rigid square array of cylinders is analyzed.

From the previously mentioned works, it is confirmed that the studies on the cantilevered pipe conveying fluid with time delay of voltage are rather limited. In this article, based on Jin's model, a time-delay control model of a standing cantilever pipe conveying fluid is developed by applying piezoelectric materials and considering the time delay of

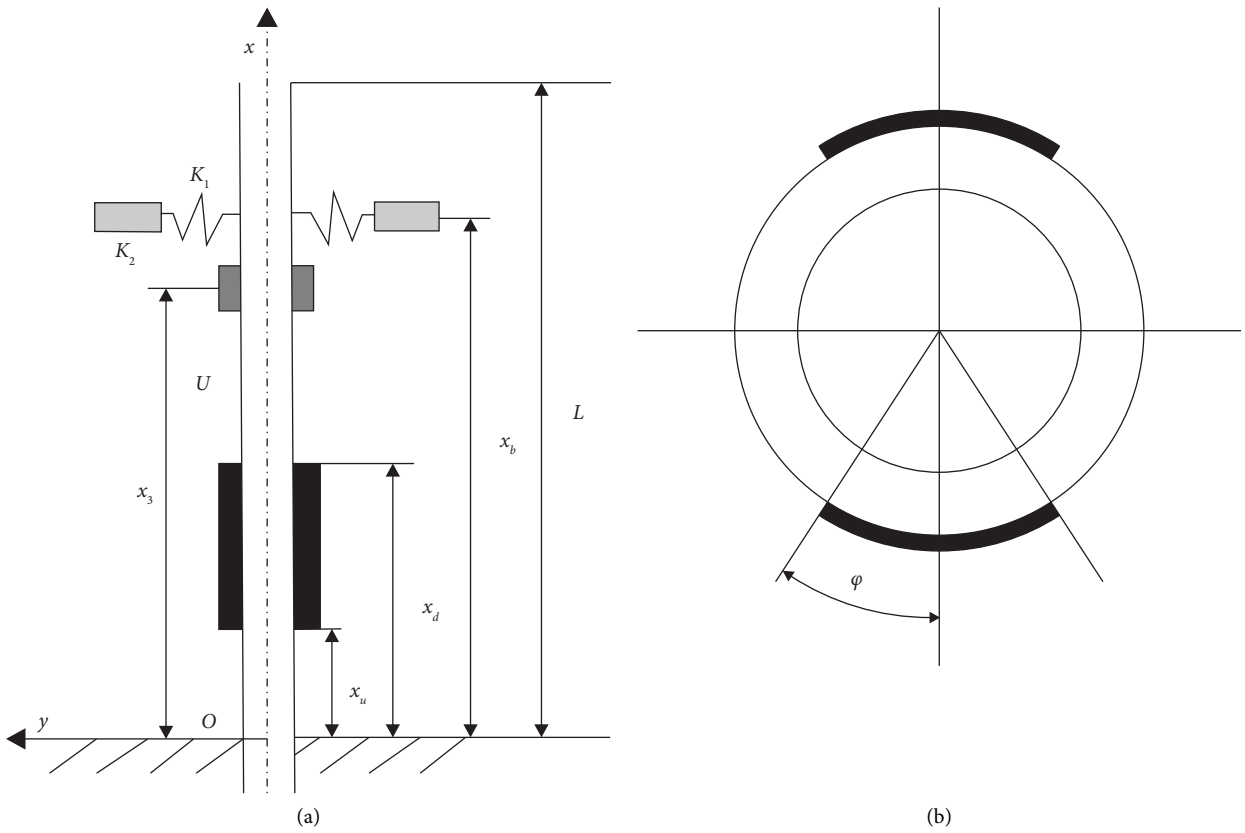

Figure 1: (a) The model of the controlled pipe conveying fluid system and (b) cross-section diagram of the pipe conveying fluid.

voltage, as shown in Figure 1. The stability of the trivial equilibrium of the nonlinear controlled system and the corresponding Hopf bifurcations appearing on the stability boundary is investigated. It should be noted that the theory of the linear part of the system is the same as the one studied by Qi and Xu [24]. The purpose of this paper is to investigate the effect of parameters such as time delay on stability and bifurcation behavior of the system after the system changes from a conventional dynamical system to a more complex time-delay dynamical system.

2. Mathematical Model and Descretized Method

The nonlinear motion equation of the controlled system is derived from the literature [12].

$$\begin{aligned} &aEI\frac{\partial^5 y}{\partial x^4 \partial t} + EI\frac{\partial^4 y}{\partial x^4} + \left[m_1U^2 + \left(m_1 + m_p\right)(L-x)g\right]\frac{\partial^2 y}{\partial x^2} + 2m_1U\frac{\partial^2 y}{\partial x \partial t} \\ &\quad -\left(m_1 + m_p\right)g\frac{\partial y}{\partial x} + \left(m_1 + m_p\right)\frac{\partial^2 y}{\partial t^2} + \left(K_1 y + K_2 y^3\right)\delta\left(x - x_b\right) \\ &\quad = \frac{\partial}{\partial x}\left\{C_m V(t)\left[\delta\left(x - x_u\right) - \delta\left(x - x_d\right)\right]\right\}, \end{aligned} \tag{1}$$

where C_m is a constant related to the physical and geometric properties of piezoelectric materials. The expression of C_m can be referred to [12].

As shown in Figure 1, the left and right surfaces of the pipe are symmetrically arranged with piezoelectric patches. It is assumed that the piezoelectric patches are ideally attached to the pipe, regardless of the influence of the mass and stiffness of the piezoelectric patches. The piezoelectric patches are surface bonded on the pipe, piezoelectric patches produce geometric deformation under controlled voltage, and equivalent bending moments are generated, which is opposite to the vibration direction of the pipe. The explanation of each notation of the system is shown in the following table. In Table 1, the parameter φ can be found in the expression of C_m which can be seen in Ref [12]. The central manifold theorem and the canonical type theory are used to

Table 1: Summary of symbols.

Notation	Explanation
EI	Flexural rigidity of the pipe
a	Coefficient of Kelvin–Voigt viscoelastic damping of the pipe material
L	Pipe length
m_p	Mass per unit length
m_1	Mass of the conveying fluid per unit length
U	Flow velocity
K_1	Stiffness of the spring of the elastic support
K_2	Stiffness of cubic spring which represents the effect of the motion constraints
x_b	Location of the constraints
x_u	Distance between the fixed end of the piezoelectric plate and the upper end of the pipeline
x_d	Distance between the fixed end of the piezoelectric plate and the lower end of the pipeline
x_3	Position coordinates of the sensor
φ	Envelope half angle of a piezoelectric plate
g	Acceleration due to gravity
$\delta(\cdot)$	Dirac delta function
$y(x,t)$	Lateral deflection of the pipe

study the stability of Hopf branching directions and branching period solution about a standing cantilever pipe conveying fluid.

Introducing the following dimensionless quantities and parameters:

$$\eta = \frac{y}{L}, \xi = \frac{x}{L}, \tau = \left(\frac{EI}{m_1 + m_p}\right)^{1/2} \frac{t}{L^2}, u = \left(\frac{m_1}{EI}\right)^{1/2} UL, \gamma = \frac{m_1 + m_p}{EI} gL^3,$$
$$\xi_b = \frac{x_b}{L}, \xi_1 = \frac{x_u}{L}, \xi_2 = \frac{x_d}{L}, \alpha = \left(\frac{EI}{m_1 + m_p}\right)^{1/2} \frac{a}{L^2}, k_1 = K_1 \frac{L^3}{EI}, k_2 = K_2 \frac{L^5}{EI}, \tag{2}$$
$$\beta = \frac{m_1}{m_1 + m_p}, C_m^* V_a^*(t^*) = \frac{LC_m}{EI} V_a(t).$$

Equation (1) can be rewritten as the following dimensionless form:

$$\alpha \dot{\eta}'''' + \eta'''' + \left[u^2 + (1-\xi)\gamma\right]\eta'' + 2\sqrt{\beta} u \dot{\eta}' - \gamma\eta' + \ddot{\eta} + \left(k_1\eta + k_2\eta^3\right)\delta(\xi - \xi_b) = C_m^* V_a^*(t^*)\left[\delta'(\xi - \xi_1) - \delta'(\xi - \xi_2)\right], \tag{3}$$

where $(\cdot) = \partial()/\partial t$, $()' = \partial()/\partial\xi$. The following equations remove the asterisk for convenience.

Equation (3) can be discretized by Galerkin's technique as follows:

$$\eta(\xi, \tau) = \sum_{r=1}^{N} \varphi_r(\xi) q_r(\tau), \tag{4}$$

where

$$\varphi_r(\xi) = \cos h\lambda_r\xi - \cos\lambda_r\xi - \frac{\sinh\lambda_r - \sin\lambda_r}{\cosh\lambda_r + \cos\lambda_r}(\sinh\lambda_r\xi - \sin\lambda_r\xi), \tag{5}$$

are the eigenfunctions of the cantilever beam and $q_r(\tau)$ are the corresponding generalized coordinate. Substituting (4) into (3) and using the Galerkin method, we obtain a four-dimensional ordinary differential equation of motion as follows:

$$\delta_{sr}\ddot{q}_r + \left(\alpha\lambda_r^4\delta_{sr} + 2\sqrt{\beta}\, u b_{sr}\right)\dot{q}_r + \left(\lambda_r^4\delta_{sr} + u^2 c_{sr} - \gamma e_{sr}\right)q_r + k_1\varphi_s(\xi_b)\varphi_r(\xi_b)q_r + k_2\varphi_s(\xi_b)\varphi_r^3(\xi_b)q_r^3 = M_s V_a(t), \tag{6}$$

where

$$b_{sr} = \int_0^1 \varphi_s\varphi_r' \mathrm{d}\xi, c_{sr} = \int_0^1 \varphi_s\varphi_r'' \mathrm{d}\xi, d_{sr} = \int_0^1 \varphi_s\xi\varphi_r'' \mathrm{d}\xi, e_{sr} = b_{sr} - c_{sr} + d_{sr}, M_s = C_m\left[\varphi_s'(\xi_2) - \varphi_s'(\xi_1)\right], \tag{7}$$

where $s, r = 1, 2, \ldots, N$ and λ_r represent the eigenvalues of the cantilever beam and δ_{sr} is Kronecker's delta function.

In this article, the driving voltage considering piezoelectric excitation adopts the displacement delay feedback strategy [26], which is denoted as follows:

$$V_a(t) = \sum_{r=1}^{N} -k_d \varphi_r(\xi_3) q_r(t-\tau), \tag{8}$$

where k_d is the displacement controller feedback gains, ξ_3 is the position coordinates of the sensor, and τ is the inherent system delay, which denoted as $-M_s k_d \varphi_r(\xi_3) = k_{sr}$.

In system (1), the flutter instability occurs in the second mode, so the first two modes of the system are intercepted by Galerkin's method. Substituting $V_a(t)$ into equation (7), we obtain

$$\begin{aligned}
&q_1 + \left(\alpha\lambda_1^4 + 2\sqrt{\beta}ub_{11}\right)\dot{q}_1 + 2\sqrt{\beta}ub_{12}\dot{q}_2 + \left(\lambda_1^4 + u^2c_{11} - \gamma e_{11}\right)q_1 + \left(u^2c_{12} - \gamma e_{12}\right)q_2 + k_1\varphi_1(\xi_b) \\
&\quad [\varphi_1(\xi_b)q_1 + \varphi_2(\xi_b)q_2] + k_2\varphi_1(\xi_b)[\varphi_1(\xi_b)q_1 + \varphi_2(\xi_b)q_2]^3 = k_{11}q_{1\tau} + k_{12}q_{2\tau}, \\
&q_2 + \left(\alpha\lambda_2^4 + 2\sqrt{\beta}ub_{22}\right)\dot{q}_2 + 2\sqrt{\beta}ub_{21}\dot{q}_1 + \left(\lambda_2^4 + u^2c_{22} - \gamma e_{22}\right)q_2 + \left(u^2c_{21} - \gamma e_{21}\right)q_1 + k_1\varphi_2(\xi_b) \\
&\quad [\varphi_1(\xi_b)q_1 + \varphi_2(\xi_b)q_2] + k_2\varphi_2(\xi_b)[\varphi_1(\xi_b)q_1 + \varphi_2(\xi_b)q_2]^3 = k_{21}q_{1\tau} + k_{22}q_{2\tau}.
\end{aligned} \tag{9}$$

Let $x_1 = q_1, x_2 = q_2, x_3 = \dot{q}_1, x_4 = \dot{q}_2$, after proper arrangement and transformation, we obtain

$$\dot{X} = AX(t) + BX(t-\tau) + F(X), \tag{10}$$

where

$$\begin{aligned}
&X = (x_1, x_2, x_3, x_4)^{\mathrm{T}}, F(X) = (0, 0, F_3, F_4)^{\mathrm{T}}, \\
&\mathbf{A} = \begin{pmatrix} 0 & 0 & 1 & 0 \\ 0 & 0 & 0 & 1 \\ a_1 & a_2 & a_3 & a_4 \\ b_1 & b_2 & b_3 & b_4 \end{pmatrix}, \mathbf{B} = \begin{pmatrix} 0 & 0 & 0 & 0 \\ 0 & 0 & 0 & 0 \\ k_{11} & k_{12} & 0 & 0 \\ k_{21} & k_{22} & 0 & 0 \end{pmatrix}, \\
&a_1 = -\left(\lambda_1^4 + u^2c_{11} - \gamma e_{11} + k_1 g_{11}\right), a_2 = -\left(u^2c_{12} - \gamma e_{12} + k_1 g_{12}\right), \\
&a_3 = -\left(\alpha\lambda_1^4 + 2\sqrt{\beta}ub_{11}\right), a_4 = -2\sqrt{\beta}ub_{12}, \\
&b_1 = -\left(u^2c_{21} - \gamma e_{21} + k_1 g_{21}\right), b_2 = -\left(\lambda_2^4 + u^2c_{22} - \gamma e_{22} + k_1 g_{22}\right), \\
&b_3 = -2\sqrt{\beta}ub_{21}, b_4 = -\left(\alpha\lambda_2^4 + 2\sqrt{\beta}ub_{22}\right), \\
&F_3 = -k_2\varphi_1(\xi_b)[\varphi_1(\xi_b)x_1 + \varphi_2(\xi_b)x_2]^3, F_4 = \frac{\varphi_2(\xi_b)F_3}{\varphi_1(\xi_b)} g_{sr} = \varphi_s(\xi_b)\varphi_r(\xi_b)(r, s = 1, 2).
\end{aligned} \tag{11}$$

3. Stability of Equilibrium with Time Delay

In the previous section, we built the model of the standing cantilever pipe conveying fluid with time delay. In this section, the stability of the system will be discussed by the eigenvalue method. The discussion of the linear part has been carried out by Qi and Xu [24]. In order to describe the Hopf bifurcation of the nonlinear systems in the next section, a simple derivation of the linear part is presented.

3.1. Solution of the Equilibrium. The equilibrium can be obtained from the following equation:

$$\begin{cases}
a_1x_1 + a_2x_2 + k_{11}x_1(t-\tau) + k_{12}x_2(t-\tau) + F3 = 0, \\
b_1x_1 + b_2x_2 + k_{21}x_1(t-\tau) + k_{22}x_2(t-\tau) + F4 = 0, \\
x_3 = 0, \\
x_4 = 0.
\end{cases} \tag{12}$$

According to Jin's method [4], three equilibriums of the system can be obtained as follows:

$$(0,0,0,0) \equiv \{\mathbf{0}\},\ (k\sqrt{c}\,,\sqrt{c}\,,0,0) \equiv +\{\mathbf{N}\},\quad (-k\sqrt{c}\,,-\sqrt{c}\,,0,0) \equiv -\{\mathbf{N}\}, \tag{13}$$

where

$$c = \frac{(a_1k + a_2 + k_{11}k + k_{12})}{b}, b = k_2 g_{11}^2 \left(k + \frac{g_{12}}{g_{11}}\right)^3,$$
$$k = \frac{a_2 + k_{12} - eb_2 - ek_{22}}{eb_1 + ek_{21} - a_1 - k_{11}} = \frac{e\lambda_2^4 + u^2(ec_{22} - c_{12}) - \gamma(ee_{22} - e_{12}) + k_{12} - ek_{22}}{\lambda_1^4 + u^2(c_{11} - ec_{21}) - \gamma(e_{11} - ee_{21}) + ek_{21} - k_{11}}. \tag{14}$$

It is clear that the solution (0, 0, 0, 0) always exists. The nonzero equilibrium exists when $c > 0$ as shown in Figure 2. The parameters are set as $\alpha = 0.005, \beta = 0.2, \gamma = 10, \xi_b = 0.82, \xi_1 = 0, \xi_2 = 0.2, \xi_3 = 0.8, C_m = 0.178$.

3.2. Stability Analysis of the Equilibrium. At the zero equilibrium, we have $O = (0,0,0,0)$. Substituting the trial solution $X = \overline{X}e^{\lambda t}$ into the linear part of (10), we obtain the characteristic equation as follows:

$$\lambda^4 + d_1\lambda^3 + d_2\lambda^2 + d_3\lambda + d_4 + \left(d_5\lambda^2 + d_6\lambda + d_7\right)e^{-\lambda\tau} + d_8e^{-2\lambda\tau} = 0, \tag{15}$$

where $d_1 = -a_3 - b_4, d_2 = -a_1 - b_2 + a_3b_4 - a_4b_3$, $d_3 = a_1b_4 - a_2b_3 + a_3b_2 - a_4b_1$, $d_4 = a_1b_2 - a_2b_1, d_5 = -k_{11} - k_{22}$, $d_6 = a_3k_{22} - a_4k_{21} - b_3k_{12} + b_4k_{11}$, and $d_7 = a_1k_{22} - a_2k_{21} - b_1k_{12} + b_2k_{11}, d_8 = k_{11}k_{22} - k_{12}k_{21}$.

3.2.1. Stability of Systems without Delay. When $\tau = 0$, (15) becomes

$$\lambda^4 + d_1\lambda^3 + (d_2 + d_5)\lambda^2 + (d_3 + d_6)\lambda + d_4 + d_7 + d_8 = 0. \tag{16}$$

Let

$$\mathbf{D} = \begin{pmatrix} d_1 & 1 & 0 & 0 \\ d_3 + d_6 & d_2 + d_5 & d_1 & 1 \\ 0 & d_4 + d_7 + d_8 & d_3 + d_6 & d_2 + d_5 \\ 0 & 0 & 0 & d_4 + d_7 + d_8 \end{pmatrix}. \tag{17}$$

Then, the Routh–Hurwitz criterion is given by

$$\mathbf{D_1} > 0, \mathbf{D_2} > 0, \mathbf{D_3} > 0, \mathbf{D_4} > 0. \tag{18}$$

If (18) holds, the equilibrium $O(0,0,0,0)$ is locally asymptotically stable.

The stability boundaries of the equilibrium x^* on the (u, k_1) plane without delay are shown in Figure 3. When the flow velocity u crosses the boundary B_H from left to right, the system loses its stability and a Hopf bifurcation occurs. Figure 4 shows the curve of an eigenvalue changing with flow velocity for the system with $\tau = 0$ and $k_1 = 20$. It can be seen that when u increases to 5.2, the system undergoes a Hopf bifurcation.

3.2.2. Stability of System with Delay. By multiplying $e^{\lambda\tau}$ on both sides of (15), we get

$$P(\lambda)e^{\lambda\tau} + Q(\lambda) + R(\lambda)e^{-\lambda\tau} = 0, \tag{19}$$

where $P(\lambda) = \lambda^4 + d_1\lambda^3 + d_2\lambda^2 + d_3\lambda + d_4, Q(\lambda) = d_5\lambda^2 + d_6\lambda + d_7$, $R(\lambda) = d_8$. By using the method of Qi and Xu [24], the corresponding critical value of time delay τ_k can be determined by

$$\cos(\omega_0\tau_k) = -\frac{(P_R - R_R)Q_R + (P_I - R_I)Q_I}{P_R^2 + P_I^2 - R_R^2 - R_I^2}, \tag{20}$$

$$\sin(\omega_0\tau_k) = \frac{(P_I + R_I)Q_R - (P_R + R_R)Q_I}{P_R^2 + P_I^2 - R_R^2 - R_I^2}, \tag{21}$$

where $P_R = \mathrm{Re}(P(i\omega)) = \omega^4 - d_2\omega^2 + d_4$, $P_I = \mathrm{Im}(P(i\omega)) = -d_1\omega^3 i + d_3\omega i$, $Q_R = \mathrm{Re}(Q(i\omega)) = -d_5\omega^2 + d_7$, $Q_I = \mathrm{Im}(Q(i\omega)) = d_6\omega i$, and $R_R = \mathrm{Re}(R(i\omega)) = d_8$, $R_I = \mathrm{Im}(R(i\omega)) = 0$.

The real and imaginary part of $(\mathrm{d}\lambda/\mathrm{d}\tau)$ at $\lambda = i\omega_0$ is given by

$$\mathrm{Re}\left[\frac{\mathrm{d}\lambda}{\mathrm{d}\tau}\right]\Big|_{\tau=\tau_k} = \frac{U_1V_1 + U_2V_2}{V_1^2 + V_2^2}, \mathrm{Im}\left[\frac{\mathrm{d}\lambda}{\mathrm{d}\tau}\right]\Big|_{\tau=\tau_k} = \frac{-U_1V_2 + U_2V_1}{V_1^2 + V_2^2}, \tag{22}$$

where

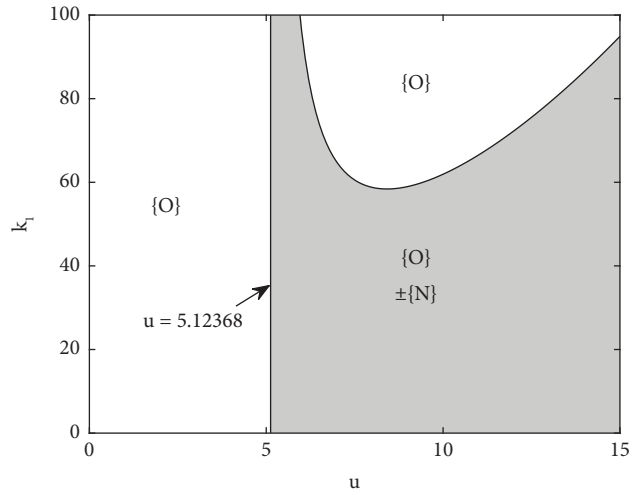

Figure 2: Existence region of nonzero equilibrium. The domain marked by the gray shadows indicates the existence of nonzero equilibria.

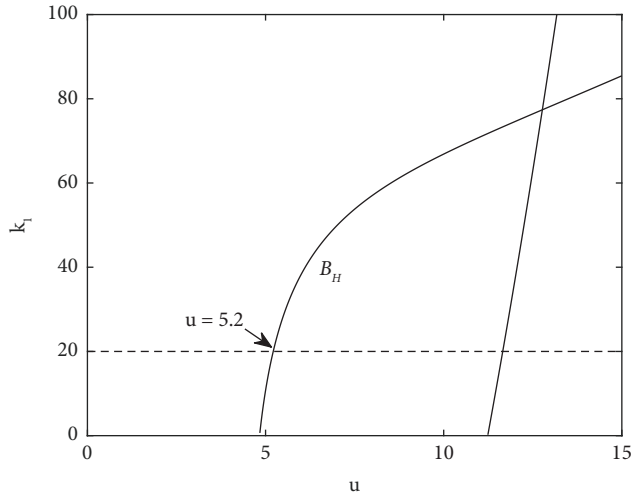

Figure 3: Stable regions of the equilibrium O on the (u, k_1) plane without delay.

$$\begin{aligned}
U_1 &= -\left(d_1\omega^4 - d_3\omega^2\right)\cos(\omega\tau_k) - \left(-\omega^5 + d_2\omega^3 - d_4\omega - d_8\omega\right)\sin(\omega\tau),\\
U_2 &= -\left(\omega^5 - d_2\omega^3 + d_4\omega - d_8\omega\right)\cos(\omega\tau) - \left(d_1\omega^4 - d_3\omega^2\right)\sin(\omega\tau),\\
V_1 &= \left(-3d_1\omega^2 + d_3 + \omega^4\tau_k - d_2\omega^2\tau_k + d_4\tau_k - d_8\tau_k\right)\cos(\omega\tau_k) + \left(4\omega^3 - 2d_2\omega + d_1\omega^3\tau_k - d_3\omega\tau_k\right)\sin(\omega\tau_k) + d_6,\\
V_2 &= \left(-4\omega^3 + 2d_2\omega - d_1\omega^3\tau_k + d_3\omega\tau_k\right)\cos(\omega\tau_k) + \left(-3d_1\omega^2 + d_3 + \omega^4\tau_k - d_2\omega^2\tau_k + d_4\tau_k + d_8\tau_k\right)\sin(\omega\tau_k) + 2d_5\omega.
\end{aligned} \tag{23}$$

If $\mathrm{Re}[d\lambda/d\tau]|_{\tau=\tau_k} > 0$, the critical roots of (19) cross the axis from left to right. If $\mathrm{Re}[d\lambda/d\tau]|_{\tau=\tau_k} < 0$, the critical roots of (19) cross the axis from right to left.

We set $k_1 = 20$ and the other parameters are the same as in Figure 2. We obtain the stability region of the equilibrium on the (u, τ) plane according to the continuity and stability switches analysis, as shown in Figure 5.

Taking the velocity $u = 5.3$ as an example, the positive real roots of (20) and (21) can be calculated as $\omega_1 \approx 11.777491, \omega_2 \approx 13.116553$ and the corresponding critical delays $\tau_1^{(k)}, \tau_2^{(k)}$ can be calculated as follows:

$$\begin{aligned}
&\tau_1^{(0)} \approx 0.141761, \tau_1^{(1)} \approx 0.675252\cdots,\\
&\tau_2^{(0)} \approx 0.456237, \tau_2^{(1)} \approx 0.935264\cdots.
\end{aligned} \tag{24}$$

Then, the sign of $\mathrm{Re}[d\lambda/d\tau]|_{\tau=\tau_k}$ can be obtained as $\mathrm{Re}[d\lambda/d\tau]|_{\tau=\tau_1^{\{0\}}} < 0$ and $\mathrm{Re}[d\lambda/d\tau]|^{\{0\}}_{\tau=\tau_2} > 0$, which means the

characteristic roots cross the imaginary axis from right to left at $\tau_1^{\{0\}}$ and from left to right at $\tau_2^{\{0\}}$.

The distribution of the eigenvalue for the delayed control system can be simulated by the MATLAB BIFTOOL package, as shown in Figure 6.

(1) When $\tau = 0$, the system has only four eigenvalues. Two of them are on the right half of the complex plane, indicating that the system is unstable, as shown in Figure 6(a).

(2) As the delay increases, it can be seen from Figures 6(b) and 6(c) that the delayed control system is unstable when $\tau = 0.14$. When $\tau = 0.15$, the system undergoes the first stability switch and becomes stable.

(3) As the delay continues to increase, it can be seen from Figures 6(d) and 6(e) that the delayed control system is stable when $\tau = 0.45$. When $\tau = 0.46$, the system undergoes the stability switch again and becomes unstable.

Time history of the controlled system with and without time delay when $u = 5.3$ is shown in Figure 7. It is found that delayed control makes the previously unstable system stable.

The stability region of the equilibrium on the (k_1, τ) plane is shown in Figure 8. By comparing Figures 5 and 8, it can be seen that k_1 can also affect the critical flow velocity of the system. When $u = 5.5$ and $k_1 = 20$, the system is stable in the delay interval [0.19, 0.41] and [0.74, 0.89]. When $u = 5.5$ and $k_1 = 35$, the system is stable in the full delay interval.

It should be noted that a Hopf bifurcation would occur on the stability boundary (the red lines in Figure 5). When the time delay τ crosses the stability boundaries shown in Figure 5, a periodic solution may appear near the equilibrium point. The stability and bifurcating direction of these periodic solutions, as well as the period of the periodic solutions, will be further analyzed in the next section.

4. Direction and Stability of the Hopf Bifurcation

In the previous section, there exists one pair of purely imaginary eigenvalues $\pm i\omega$ on the stability boundary of the equilibrium. Consequently, a Hopf bifurcation will arise at $\tau = \tau_k$. In this section, the direction of Hopf bifurcation and the stability of bifurcation periodic solutions will be analyzed. Our approach is the paradigm theory and central flow type theorem proposed by Hassan et al. [27]. For simplicity, let $\tau = \tau_k + \mu, \mu \in R$. Then, $\mu = 0$ is the corresponding Hopf bifurcation point.

For $\phi \in C = C([-\tau, 0], R^4)$, we assume that

$$L_\mu \phi = \mathbf{A}\phi(0) + \mathbf{B}\phi(-\tau), \tag{25}$$

where matrices $\mathbf{A}$ and $\mathbf{B}$ are defined in (10). According to the Riesz representation theorem, there exists a bounded variation function $\eta(\theta, \mu)$ such that

$$L_\mu \phi = \int_{-\tau}^{0} \mathrm{d}\eta(\theta, \mu)\phi(\theta) \text{for} \quad \phi \in C[-\tau, 0] \longrightarrow R^4, \tag{26}$$

where we choose the following expression to satisfy the equation:

$$\eta(\theta, \mu) = \begin{cases} \mathbf{A}, & \theta = 0, \\ \mathbf{0}, & \theta \in (-\tau, 0), \\ -\mathbf{B}, & \theta = -\tau. \end{cases} \tag{27}$$

For $\phi \in C = C([-\tau, 0], R^4)$, we define

$$S(\mu)\phi(\theta) = \begin{cases} \dfrac{\mathrm{d}\phi(\theta)}{\mathrm{d}\theta}, & \theta \in [-\tau, 0], \\ \displaystyle\int_{-\tau}^{0} \mathrm{d}\eta(\theta, \mu)\phi(\theta) & \theta = 0, \end{cases} \tag{28}$$

$$T(\mu)\phi(\theta) = \begin{cases} 0, & \theta \in [-\tau, 0], \\ F(\phi(0)), & \theta = 0, \end{cases} \tag{29}$$

then, (10) can be rewritten as follows:

$$\dot{X}_t = S(\mu)X_t + T(\mu)X_t, \tag{30}$$

where $X_t(\theta) = X(t + \theta)$ and $\theta \in [-\tau, 0]$.

We define the corresponding adjoint operator S^* of the operator T

$$S^*(\mu)\psi(s) = \begin{cases} -\dfrac{\mathrm{d}\psi(s)}{\mathrm{d}s}, & s \in (0, \tau), \\ \displaystyle\int_{-\backslash tau}^{0} \mathrm{d}\eta^T(s, \mu)\psi(-s), & s = 0, \end{cases} \tag{31}$$

and a bilinear form of vectors

$$\langle \psi(s), \phi(\theta) \rangle = \overline{\psi}^T(0)\phi(0) - \int_{\theta=-\tau}^{0} \int_{\xi=0}^{\theta} \overline{\psi}^T(\xi - \theta)\mathrm{d}\eta(\theta)\phi(\xi)\mathrm{d}\xi, \tag{32}$$

where $\eta(\theta) = \eta(\theta, 0)$.

According to the discussion in the previous section, $\pm i\omega$ are the eigenvectors of $S(0)$ and $S^*(0)$, respectively. Next, we need to figure out the eigenvector of the operator $S(0)$ and the eigenvector of $S^*(0)$. Based on the definition of $S(0)$ and $S^*(0)$, we obtain

$$q(\theta) = \begin{pmatrix} 1 & v_1 & v_2 & v_3 \end{pmatrix}^T e^{i\omega\theta}, \theta \in [-\tau, 0]. \tag{33}$$

$$q^*(s) = G\begin{pmatrix} 1 & v_1^* & v_2^* & v_3^* \end{pmatrix}^T e^{i\omega s}, s \in [0, \tau], \tag{34}$$

where

$$
\begin{aligned}
v_1 &= -\frac{a_1 + a_3\omega i + \omega^2 + k_{11}e^{-i\omega\tau_k}}{a_2 + a_4\omega i + k_{12}e^{-i\omega\tau_k}},\\
v_2 &= i\omega,\\
v_3 &= i\omega v_1,\\
v_1^* &= \frac{\left(\omega^3 - a_3\omega^2 i - b_4\omega^2 i - a_1 b_4 i + a_4 b_1 i - a_3 b_4\omega + a_4 b_3\omega + a_4 k_{21}e^{i\omega\tau_k} i - b_4 k_{11}e^{i\omega\tau_k} i + k_{11}\omega e^{i\omega\tau_k}\right)}{\left(a_1 b_3 i - a_3 b_1 i + b_1\omega - a_3 k_{21}e^{i\omega\tau_k} i + b_3 k_{11}e^{i\omega\tau_k} + k_{21}\omega e^{i\omega\tau_k}\right)},\\
v_2^* &= -\frac{b_1 - b_3\omega i + k_{21}e^{i\omega\tau_k}}{a_3 b_1 - a_1 b_3 + b_1\omega i + a_3 k_{21}e^{i\omega\tau_k} - b_3 k_{11}e^{i\omega\tau_k} + k_{21}\omega e^{i\omega\tau_k} i},\\
v_3^* &= \frac{a_1 + k_{11}e^{i\omega\tau_k} + \omega^2 - a_3\omega i}{a_3 b_1 - a_1 b_3 + b_1\omega i + a_3 k_{21}e^{i\omega\tau_k} - b_3 k_{11}e^{i\omega\tau_k} + k_{21}\omega e^{i\omega\tau_k} i}.
\end{aligned}
\tag{35}
$$

From $\langle q^*(s), q(\theta)\rangle = 1$, we obtain $\overline{G} = [1 + \overline{v}_1^* v_1 + \overline{v}_2^* v_2 + \overline{v}_3^* v_3 + (k_{11}\overline{v}_2^* + k_{21}\overline{v}_3^*)\tau_k e^{-i\omega\tau_k} + (k_{12}\overline{v}_2^* + k_{22}\overline{v}_3^*)v_1\tau_k e^{-i\omega\tau_k}]^{-1}$.

According to the algorithm of Hassard et al. [27], we calculate the coordinate quantity describing the central manifold C_0 when $\mu = 0$. We assume that X_t is a solution of (30) and assume that

$$
\begin{cases}
z(t) = \langle q^*, X_t\rangle,\\
W(t,\theta) = X_t(\theta) - zq - \overline{z}\overline{q}.
\end{cases}
\tag{36}
$$

On the central manifold C_0, the following expression holds:

$$
W(z,\overline{z},\theta) = W_{20}(\theta)\frac{z^2}{2} + W_{11}(\theta)z\overline{z} + W_{02}(\theta)\frac{\overline{z}^2}{2} + \cdots,
\tag{37}
$$

where z and $\overline{z}$ are the local coordinates of the central manifold C_0 along the direction q^* and $\overline{q}^*$, respectively. Known that X_t is the solution of (30) and since $\mu = 0$, we have

$$
\dot{z}(t) = \langle q^*, \dot{X}_t\rangle = i\omega z + \overline{q}^{*T}(0)F(z,\overline{z}),
\tag{38}
$$

Equation (38) can be rewritten as follows:

$$
\dot{z}(t) = i\omega z + g(z,\overline{z}),
\tag{39}
$$

where

$$
g(z,\overline{z}) = g_{20}\frac{z^2}{2} + g_{11}z\overline{z} + g_{02}\frac{\overline{z}^2}{2} + g_{21}\frac{z^2\overline{z}}{2} + \cdots.
\tag{40}
$$

Notice that $X_t(\theta) = zq(\theta) + \overline{z}\overline{q}(\theta) + W(t,\theta)$, we obtain

$$
\begin{cases}
x_{1t}(0) = z + \overline{z} + W_{20}^{(1)}(0)\dfrac{z^2}{2} + W_{11}^{(1)}(0)z\overline{z} + W_{02}^{(1)}(0)\dfrac{\overline{z}^2}{2} + \cdots\\
x_{2t}(0) = zv_1 + \overline{z}\overline{v}_1 + W_{20}^{(2)}(0)\dfrac{z^2}{2} + W_{11}^{(2)}(0)z\overline{z} + W_{02}^{(2)}(0)\dfrac{\overline{z}^2}{2} + \cdots\\
x_{3t}(0) = zv_2 + \overline{z}\overline{v}_2 + W_{20}^{(3)}(0)\dfrac{z^2}{2} + W_{11}^{(3)}(0)z\overline{z} + W_{02}^{(3)}(0)\dfrac{\overline{z}^2}{2} + \cdots\\
x_{4t}(0) = zv_2 + \overline{z}\overline{v}_3 + W_{20}^{(4)}(0)\dfrac{z^2}{2} + W_{11}^{(4)}(0)z\overline{z} + W_{02}^{(4)}(0)\dfrac{\overline{z}^2}{2} + \cdots.
\end{cases}
\tag{41}
$$

According to the literature [27], the critical properties of bifurcation periodic solutions are determined by the following parameters:

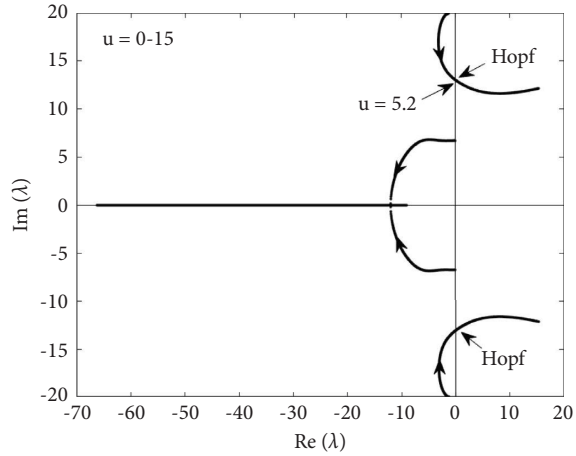

Figure 4: Eigenvalue evolutions of the equilibrium {**O**} for $k_1 = 20$.

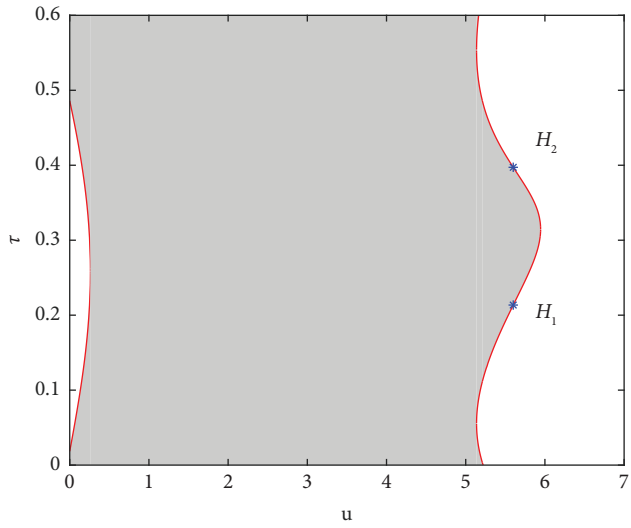

Figure 5: Stable regions of the equilibrium x^*. The stable regions are marked by the gray shadows, and the points H_1 and H_2 represent the generic Hopf bifurcation point.

$$c_1(k_c, \tau_k) = \frac{i}{2\omega}\left(g_{20}g_{11} - 2|g_{11}|^2 - \frac{|g_{02}|^2}{3}\right) + \frac{g_{21}}{2},$$

$$\mu_2 = -\frac{\mathrm{Re}\{c_1(\tau_k)\}}{\mathrm{Re}\{\lambda'(\tau_k)\}}, \tag{42}$$

$$\beta_2 = 2\mathrm{Re}\{c_1(\tau_k)\},$$

$$T_2 = -\frac{\mathrm{Im}\{c_1(\tau_k)\} + \mu_2\mathrm{Im}\{\lambda'(\tau_k)\}}{\omega}.$$

Obviously, we need to calculate the expressions of g_{20}, g_{11}, g_{02}, and g_{21}. Substituting $F(X)$ and (41) into (38) and comparing the same order of terms, we obtain the expressions of $g_{ij}{}'s$ as follows:

$$g_{20} = g_{11} = g_{02} = 0,$$

$$g_{21} = 2\overline{G}\{-k_2\varphi_1(\xi_b)[3\varphi_1^2(\xi_b)\varphi_2(\xi_b)(\overline{v}_1 + 2v_2) + 3\varphi_1(\xi_b)\varphi_2^2(\xi_b)(v_1^2 + 2v_1\overline{v}_1) + 3\varphi_1^3(\xi_b)3\varphi_2^3(\xi_b)v_1^2\overline{v}_1] \tag{43}$$

$$\overline{v}_2^* - k_2\varphi_2(\xi_b)[3\varphi_1^2(\xi_b)\varphi_2(\xi_b)(\overline{v}_1 + 2v_2) + 3\varphi_1(\xi_b)\varphi_2^2(\xi_b)(v_1^2 + 2v_1\overline{v}_1) + 3\varphi_1^3(\xi_b) + 3\varphi_2^3(\xi_b)v_1^2\overline{v}_1]\overline{v}_3^*\}.$$

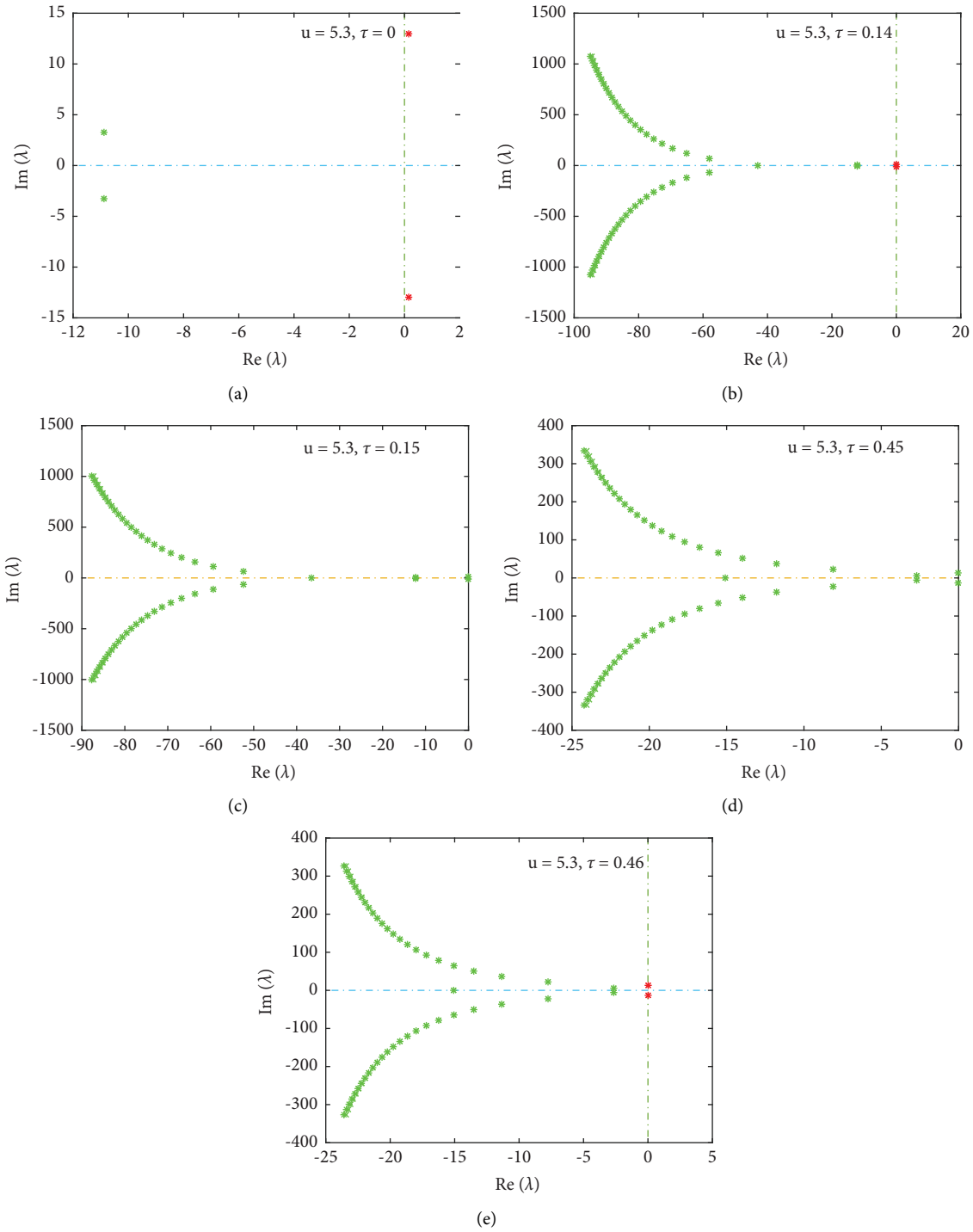

Figure 6: Distribution of eigenvalues for the delayed control system.

According to the analysis, the following theorem can be obtained:

Theorem 1. *[27]The direction of the Hopf bifurcation and the stability of the bifurcation period solution are determined by the signs of μ_2 and β_2 in (42). If $\mu_2 > 0\,(\mu_2 < 0)$, the Hopf bifurcation is supercritical (subcritical). Moreover, if $\beta_2 < 0\,(\beta_2 > 0)$, the bifurcation period solution is stable (unstable). The value of T_2 determines the period of the bifurcated periodic solution, and if $T_2 > 0\,(T_2 < 0)$, the period increases (decreases).*

In order to verify the results of the theorem, taking the velocity $u = 5.6$ as an example, the positive real roots of (20) and (21) can be calculated as $\omega_1 \approx 11.377791, \omega_2 \approx 12.997710$ and the corresponding critical delays $\tau_1^{(k)}, \tau_2^{(k)}$ can be calculated as follows:

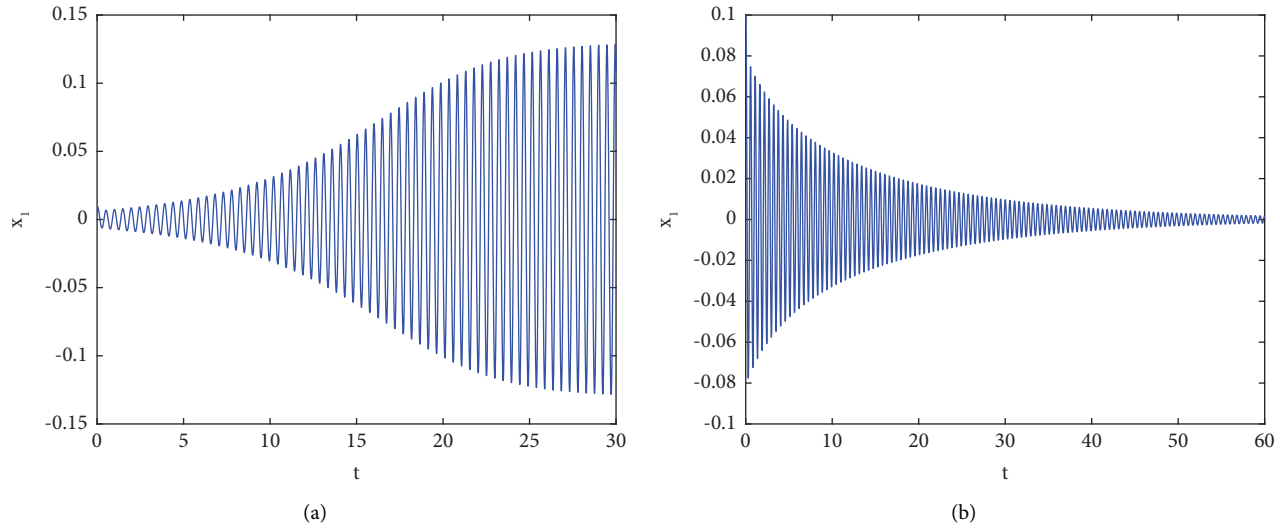

Figure 7: Time history of the controlled system. (a) $(u, \tau) = (5.3, 0)$ with the initial values $(x_1(0), x_2(0), x_3(0), \text{and } x_4(0)) = (0.01, 0, 0, 0)$ and (b) $(u, \tau) = (5.3, 0.15)$ with the initial values $(x_1(0), x_2(0), x_3(0), \text{and } x_4(0)) = (0.1, 0, 0, 0)$.

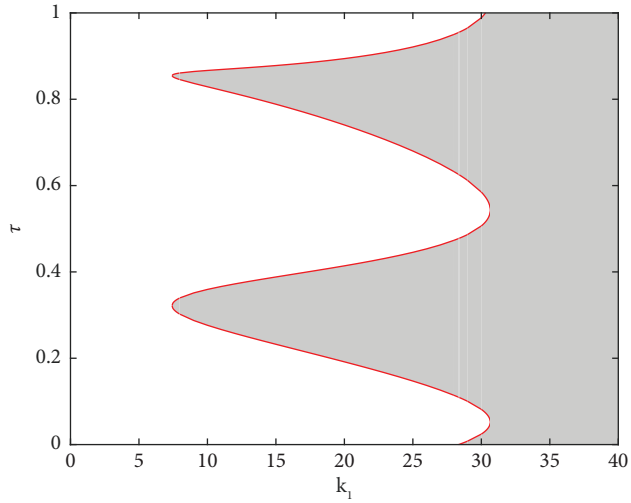

Figure 8: Stable regions of the equilibrium x^* when $u = 5.5$. The stable regions are marked by the gray shadows.

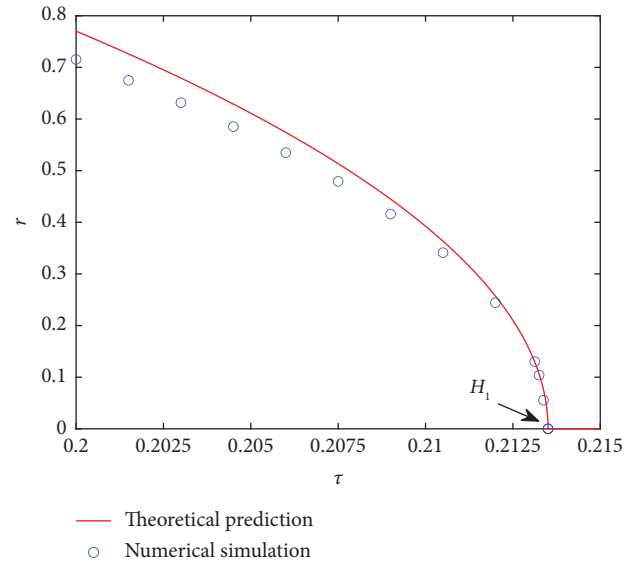

Figure 9: Bifurcation diagram near the Hopf bifurcation point H_1 in Figure 6. The Y-axis r represents the average radius of the periodic orbit, i.e., $r = \sqrt{x_1^2 + x_2^2 + x_3^2 + x_4^2}$.

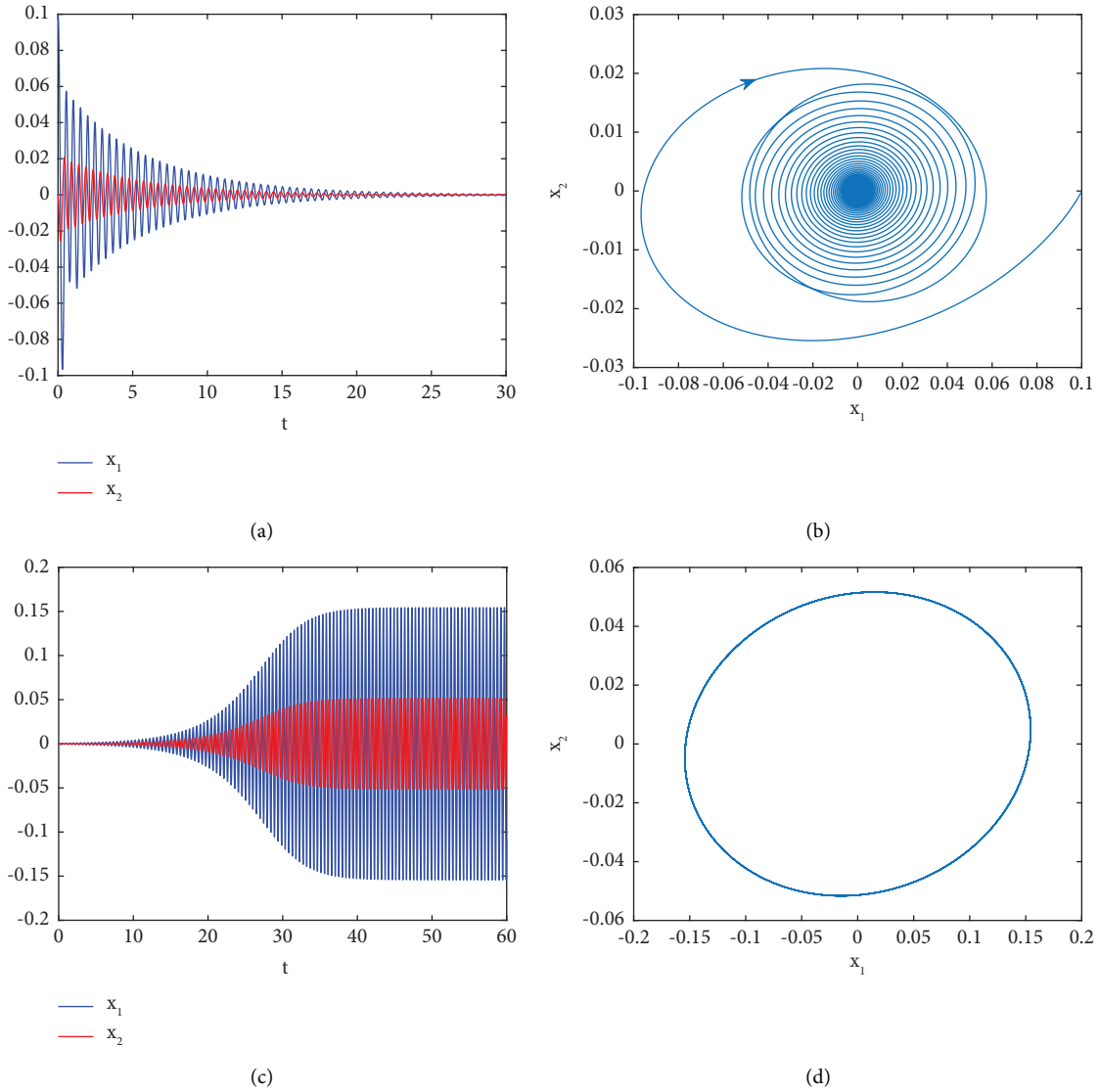

FIGURE 10: The phase diagram and response diagram near the generic Hopf bifurcation point H_2 are shown in Figure 6. (a) $(u, \tau) = (5.6, 0.38)$ with the initial values $(x_1(0), x_2(0), x_3(0)$, and $x_4(0)) = (0.1, 0, 0, 0)$, (b) the phase diagram corresponding to (a), (c) $(u, \tau) = (5.6, 0.42)$ with the initial values $(x_1(0), x_2(0), x_3(0)$, and $x_4(0)) = (0.001, 0, 0, 0)$, and (d) the phase diagram corresponding to (c).

$$\tau_1^{(0)} \approx 0.213505, \tau_1^{(1)} \approx 0.765738\cdots$$
$$\tau_2^{(0)} \approx 0.397255, \tau_2^{(1)} \approx 0.880662\cdots. \quad (44)$$

As shown in Figure 5, when the time delay increases to the critical value $\tau_1^{(0)}$ in the case of $u = 5.6$, which is marked as the point H_1, the equilibrium gains its stability. The corresponding parameter values in (42) are calculated as $\mu_2 \approx -5.7$, $\beta_2 \approx -127.7$, and $T_2 \approx -1.6$. According to Theorem 3.1, the Hopf bifurcation is subcritical, and the bifurcating periodic solution for $\tau < \tau_1^{(0)}$ is stable. We set $k_2 = 100$, the other parameters are the same as in Figure 5, and we obtain the corresponding bifurcation diagram near the Hopf bifurcation point H_1, as shown in Figure 9.

The fourth-order Runge–Kutta method is used to numerically simulate the periodic orbit amplitudes and compare with the theoretical predictions, and the results are in good agreement. The average radius of the bifurcating periodic orbit [28] can be theoretically determined as $r \approx \delta\sqrt{-\mathrm{Re}\{\lambda'(\tau_k)\}(\tau - \tau_k)/\mathrm{Re}\{c_1(\tau_k)\}}$. Here, $= 1/2\pi \int_0^{2\pi} \sqrt{(e^{i\theta} + e} \ - i\theta)^2 + (e^{i\theta}v_1 + e^{-i\theta}\overline{v}_1)^2 + (e^{i\theta}v_2 + \ e^{-i\theta}\overline{v}_2)^2 + (e^{i\theta}v_3 + e^{-i\theta}\overline{v}_3)^2 d\theta$. When the delay exceeds the critical value $\tau_2^{(0)}$, which is marked as the point H_2, the equilibrium loses its stability. The corresponding parameter values in (42) are calculated as $\mu_2 \approx 3.6$, $\beta_2 \approx -67.3$, and $T_2 \approx -2.8$. According to Theorem 3.1, the Hopf bifurcation is supercritical and the bifurcating periodic solution for $\tau > \tau_2^{(0)}$ is stable. The phase diagram and response diagram before and after the bifurcation are shown in Figure 10. Figure 10(a) shows that the vibration of the pipe conveying fluid before the bifurcation is stable. Figure 10(b) is the phase diagram corresponding to Figure 10(a), and it can be seen that the

pipe conveying fluid tends to a stable equilibrium. Figure 10(c) shows that the pipe conveying fluid after bifurcation is in stable periodic motion. Moreover, the stable bifurcating periodic orbit is shown in Figure 10(d).

5. Conclusion

In this article, a time-delay-controlled strategy was used to actively control the flutter of a standing cantilever pipe conveying fluid subject to linear springs and cubic nonlinear constraints. The motion equation is built with motion-limiting constraints and elastic support by applying piezoelectric materials and considering the time delay of voltage. The motion equation is discretized into ordinary differential equations by the Galerkin method. A stability analysis of the equilibrium point with three parameters is obtained. The stability analysis of the equilibrium of the controlled system was performed by studying the characteristic equation and stability switches. The central manifold theorem and the canonical type theory are used to study the stability of Hopf branching directions and branching period solutions. The results show that the delayed feedback control strategy can effectively improve the critical velocity of the pipe and effectively control the flutter of the nonlinear system. The results between the theoretical analysis and the numerical simulation show a good agreement, indicating the effectiveness of the control strategy.

Data Availability

The data used to support the findings of this study can be obtained from the corresponding author upon reasonable request.

Conflicts of Interest

The authors declare that they have no conflicts of interest.

Acknowledgments

The research was partially supported by the National Natural Science Foundation of China (grant number 11872043) and the Opening Project of Sichuan Province University Key Laboratory of Bridge Nondestruction Detecting and Engineering Computing (2022QYY06). The authors thank the anonymous reviewers for their helpful suggest.

References

[1] M. P. Païdoussis and N. T. Issid, "Dynamic stability of pipes conveying fluid," *Journal of Sound and Vibration*, vol. 33, no. 3, pp. 267–294, 1974.

[2] M. P. Païdoussis, G. X. Li, and F. C. Moon, "Chaotic oscillations of the autonomous system of a constrained pipe conveying fluid," *Journal of Sound and Vibration*, vol. 135, no. 1, pp. 1–19, 1989.

[3] M. P. Païdoussis, G. X. Li, and R. H. Rand, "Chaotic motions of a constrained pipe conveying fluid: comparison between simulation, analysis, and experiment," *Journal of Applied Mechanics*, vol. 58, no. 2, pp. 559–565, 1991.

[4] J. D. Jin, "Stability and chaotic motions of a restrained pipe conveying fluid," *Journal of Sound and Vibration*, vol. 208, no. 3, pp. 427–439, 1997.

[5] L. Wang and Q. Ni, "A note on the stability and chaotic motions of a restrained pipe conveying fluid," *Journal of Sound and Vibration*, vol. 296, no. 4-5, pp. 1079–1083, 2006.

[6] M. Stangl, J. Gerstmayr, and H. Irschik, "An alternative approach for the analysis of nonlinear vibrations of pipes conveying fluid," *Journal of Sound and Vibration*, vol. 310, no. 3, pp. 493–511, 2008.

[7] M. H. Ghayesh, M. P. Païdoussis, and M. Amabili, "Nonlinear dynamics of cantilevered extensible pipes conveying fluid," *Journal of Sound and Vibration*, vol. 332, no. 24, pp. 6405–6418, 2013.

[8] Z. Y. Liu, L. Wang, and X. P. Sun, "Nonlinear forced vibration of cantilevered pipes conveying fluid," *Acta Mechanica Solida Sinica*, vol. 31, no. 1, pp. 32–50, 2018.

[9] A. K. Bajaj, P. R. Sethna, and T. S. Lundgren, "Hopf bifurcation phenomena in tubes carrying a fluid," *SIAM Journal on Applied Mathematics*, vol. 39, no. 2, pp. 213–230, 1980.

[10] J. D. Jin, Y. Lin, and G. S. Zou, "Flutter and chaotic motions of a cantilevered pipe conveying fluid," *Journal of Vibration Engineering*, vol. 10, no. 3, pp. 68–74, 1997.

[11] J. D. Jin, G. S. Zou, and Y. F. Zhang, "Bifurcations and chaotic motions of a cantilevered pipe conveying fluid," *Theoretical and Applied Mechanics*, vol. 34, no. 6, pp. 863–873, 2002.

[12] G. S. Zou, J. D. Jin, and B. C. Wen, "Adaptive vibration control of a cantilevered pipe conveying fluid," *China Mechanical Engineering*, vol. 16, no. 7, pp. 626–629, 2005.

[13] J. D. Jin and G. S. Zou, "Bifurcations and chaotic motions in the autonomous system of a restrained pipe conveying fluid," *Journal of Sound and Vibration*, vol. 260, no. 5, pp. 783–805, 2003.

[14] Y. Modarres-Sadeghi, M. P. Païdoussis, and C. Semler, "Three-dimensional oscillations of a cantilever pipe conveying fluid," *International Journal of Non-linear Mechanics*, vol. 43, no. 1, pp. 18–25, 2008.

[15] K. Yamashita, N. Nishiyama, K. Katsura, and H. Yabuno, "Hopf-Hopf interactions in a spring-supported pipe conveying fluid," *Mechanical Systems and Signal Processing*, vol. 152, Article ID 107390, 2021.

[16] Y. H. Lin and C. L. Chu, "Active flutter control of a cantilever tube conveying fluid using piezoelectric actuators," *Journal of Sound and Vibration*, vol. 196, no. 1, pp. 97–105, 1996.

[17] Y. K. Tsai and Y. H. Lin, "Adaptive modal vibration control of a fluid-conveying cantilever pipe," *Journal of Fluids and Structures*, vol. 11, no. 5, pp. 535–547, 1997.

[18] S. A. Fazelzadeh and B. Yazdanpanah, "Active Flutter Suppression of Thin-Walled Cantilever Functionally Graded Piezoelectric Pipes Conveying Fluid," in *Proceedings of the 20th Annual International Conference on Mechanical Engineering-Isme2012*, pp. 1–4, Shiraz University, School of Mechanical Engineering, Shiraz, Iran, May, 2012.

[19] B. Abbasnejad, R. Shabani, and G. Rezazadeh, "Stability analysis of a piezoelectrically actuated micro-pipe conveying fluid," *Microfluidics and Nanofluidics*, vol. 19, no. 3, pp. 577–584, 2015.

[20] G. Wang and J. Shen, "Flutter instabilities of cantilevered piezoelectric pipe conveying fluid," *Journal of Intelligent Material Systems and Structures*, vol. 30, no. 4, pp. 606–617, 2019.

[21] H. Dai, Y. He, K. Zhou, Z. Peng, L. Wang, and P. Hagedorn, "Utilization of nonlinear vibrations of soft pipe conveying fluid for driving underwater bio-inspired robot," *Applied*

Mathematics and Mechanics, vol. 43, no. 7, pp. 1109–1124, 2022.

[22] H. Sugimoto, A. Horiuchi, and K. Kawasaki, "A new repetitive control and its characteristics," in *Proceedings of the SICEAnnual Conference*, vol. 2, pp. 2261–2266, Fukui, Japan, August, 2003.

[23] B. M. Mirkin and P. O. Gutman, "Adaptive control of linear time delay systems," in *Proceedings of the 2004 American Control Conference*, vol. 2, pp. 1241–1246, Massachusetts: Boston, June, 2004.

[24] H. H. Qi and J. Xu, "Delayed feedback control for flutter in the pipe conveying fluid," *Journal of Vibration Engineering*, vol. 22, no. 6, pp. 576–582, 2009.

[25] L. Wang and Q. Ni, "Hopf bifurcation and chaotic motions of a tubular cantilever subject to cross flow and loose support," *Nonlinear Dynamics*, vol. 59, no. 1-2, pp. 329–338, 2010.

[26] J. Peng, G. Zhang, M. Xiang, H. Sun, X. Wang, and X. Xie, "Vibration control for the nonlinear resonant response of a piezoelectric elastic beam via time-delayed feedback," *Smart Materials and Structures*, vol. 28, no. 9, Article ID 095010, 2019.

[27] B. D. Hassard, N. D. Kazarinoff, and Y. H. Wan, *Theory and Applications of Hopf Bifurcation*, Cambridge University Press, Cambridge, 1981.

[28] S. Deng, J. Ji, S. Yin, and G. Wen, "Multistability in the centrifugal governor system under a time-delay control strategy," *Journal of Computational and Nonlinear Dynamics*, vol. 14, no. 11, Article ID 111010, 2019.